ISACHI: Integrated Segmentation and Alignment Correction for Heart Images

Benjamin Villard(✉), Ernesto Zacur, and Vicente Grau

Institute of Biomedical Engineering, University of Oxford,
Old Road Campus Research Building, Oxford, UK
benjamin.villard@eng.ox.ac.uk

Abstract. We address the problem of cardiovascular shape representation from misaligned Cardiovascular Magnetic Resonance (CMR) images. An accurate 3D representation of the heart geometry allows for robust metrics to be calculated for multiple applications, from shape analysis in populations to precise description and quantification of individual anatomies including pathology. Clinical CMR relies on the acquisition of heart images at different breath holds potentially resulting in a misaligned stack of slices. Traditional methods for 3D reconstruction of the heart geometry typically rely on alignment, segmentation and reconstruction independently. We propose a novel method that integrates simultaneous alignment and segmentation refinements to realign slices producing a spatially consistent arrangement of the slices together with their segmentations fitted to the image data.

Keywords: Computational geometry · Slice misalignment · CMR

1 Introduction

Current research in Cardiovascular Magnetic Resonance (CMR) images is moving towards three dimensional (3D) applications, with 3D geometrical models used for various purposes, such as diagnosis, surgical planning, patient risk stratification, or device innovation [1,2]. To quantitatively assess cardiac functions, clinicians typically segment CMR slices in 2D, which are then used for the calculation of relevant 3D parameters such as volumes, ejection fraction, or myocardial mass. 3D reconstructions also allow for more sophisticated tools such as shape analysis, multi-modality fusion, or mechanical and electrophysiological simulations [3,4]. In order to accurately preserve the underlying anatomy, information obtained from magnetic resonance imaging (MRI) acquisitions needs to be spatially consistent in 3D. However, spatial inconsistencies are common due to various artefacts including patient motion inside the scanner. In CMR, the acquisition of slices at different breath holds and the natural cardiac motion introduces additional artifacts, which may introduce distortion in the generated 3D models and the subsequent quantification. Different methods can be used

M. Pop et al. (Eds.): STACOM 2018, LNCS 11395, pp. 171–180, 2019.
https://doi.org/10.1007/978-3-030-12029-0_19

to limit those artefacts: at acquisition via the use of respiratory gating [5], for example, or more clinically relevant, through image processing methods after acquisition.

Current methods for generating personalised CMR mesh models typically involve the sequential steps of misalignment correction, segmentation and interpolation. Typically, misalignments between slices are first corrected for, after which the segmented contours, obtained using manual or (semi-) automated methods, are used to create the mesh. However the sparsity of the data make registration and interpolation methods sensitive to local minima requiring strong prior assumptions. With contouring protocols extracting the object of interest in 2D, these contours suffer from spatially inconsistency [6], which is further extended by segmentation variability. Our aim is to develop an integrated method that combines the alignment of slices and a fine correction of the contours, for which an initial segmentation is obtained using any state of the art algorithm, in order to arrange the segmented data consistently in a 3D environment, ultimately, leading to accurate geometrical meshes representing the heart anatomy.

There exists prior work that simultaneously correct for spatial misalignment and quantify morphological and dynamic information [7]. However, [7] rely on prior shape models which can bias the alignment. Marchesseau *et al.* [8], use all of the multi-frame segmentations from cardiac data to generate an average mesh which they deform using estimated transformation obtained via registration, to quantify regional volume change. To our knowledge, only one prior work has attempted to achieve the integration of segmentation, spatial correction and 3D reconstruction from CMR images [9,10]. Paiement *et al.* demonstrate a technique that integrates these steps, making use of level sets to automatically segment and construct a 3D surface of the left ventricle on which they perform the alignment correction. By constraining the level sets to grow by using the combined information found in the intersecting slices, they allow the integration of the alignment and level set's segmentation. Validation is performed on registration results but not, to our knowledge, on the segmentation.

We propose a novel methodology to correct for spatially inconsistent contours, allowing for a subsequent precise *patient-specific* surface mesh reconstruction, whilst aligning the image stacks. The method makes use of long axis (LAX) and short axis (SAX) views to resolve the alignment. Our approach is image driven, and does not necessitate any expert contouring, although an initial segmentation is required. By combining information from both the alignment as well as the segmentation steps in an integrated manner, we are able to obtain an accurate shape that is spatially consistent with the information from the images. By using an initial mesh, generated by using automatically segmented contours via a convolutional neural network (CNN), we compute image derived forces that rigidly transform the image poses whilst deforming the segmentations towards image edges. The resulting segmentation combines both global and local information from the stack of short axis images as well as from the long axis view, aiming at maximizing consistency at the intersection of slices.

2 Proposed Framework

Our proposed method, ISACHI (Integrated Segmentation and Alignment Correction for Heart Images), aims to correct for segmentation errors in order to obtain 3D spatially consistent segmentations, allowing us to produce an accurate, and spatially consistent surface mesh. This is done by relying on an image-derived metric. Many different metrics would work in this context, as long as they are able to guide the segmentation towards the likely location of contours in each of the intersecting images, with our proposed framework incorporating 3D consistency. The image-derived metric is introduced in the shape of an *edgemap*, with areas with high *edgness* reflecting borders and edges. In our experiments we demonstrate the use of a deep learning approach for this initial segmentation, without affecting the generality of the framework.

2.1 Automatic Segmentation

Our method requires an initial segmentation to create an initial 3D surface mesh "$\mathcal{M}$" using the method described in [11,12]. The segmentation can be obtained in many ways; algorithmically via modern convolutional neural networks (CNN), for example, or via manual contouring. In order to render our method fully automatic, we used a U-Net CNN based on [13] as they have recently been shown to provide state-of-the-art segmentation results [14] and can work well on limited training data. While other potentially more accurate methods such as ResNet [15], our aim in this paper is to demonstrate the accuracy of the method and its robustness to the initial segmentation.

Since most current CNN segmentation techniques, including the one we use here, rely on 2D segmentation, the aforementioned 3D inconsistencies remain. While 3D CNN segmentation algorithms have been recently proposed [16–18], these require access to a large well aligned ground-truth-labelled volumetric cardiac dataset, as well as require high computational and memory requirements [16]. Standard clinical CMR does not provide 3D consistent data, and datasets should be considered as an independent collection of 2D slices.

2.2 Methodology

We compute the line intersections between all cross-sectional planes and obtain the points where the lines intersect with the generated mesh. Let l_{ij} be the line intersection between two planes containing contours C_i and C_j, with $i, j \in [1...N]$, N being the total number of contours. Let S_i be the plane containing contour C_i, with $\{S\}$ is the set of all planes containing respective contours. We denote $l_{ij} = S_i \bigcap S_j$; with $i < j$, or $l_{ij} \equiv l_{ji}$. Let $\{P^n\}$ be a set of sampled points where the lines l_{ij}, intersect with the mesh $\mathcal{M}$, i.e. $\{P^n\} = \{\mathcal{M} \bigcap l_{ij}, i < j\}$ with $n \in [1...T]$ and T being equal to the maximum amount of intersection points. At these points *patches* are created. Let D^n be the patch lying on the plane tangent to $\mathcal{M}$ with center P^n. Thus, $D^n = (\top_{P^n}(\mathcal{M})) \bigcap (B_{P^n} R)$, where B is a sphere of radius R and $\top_{P^n}(\mathcal{M})$ the tangent to $\mathcal{M}$ at point P^n. Let X_i be a segment of

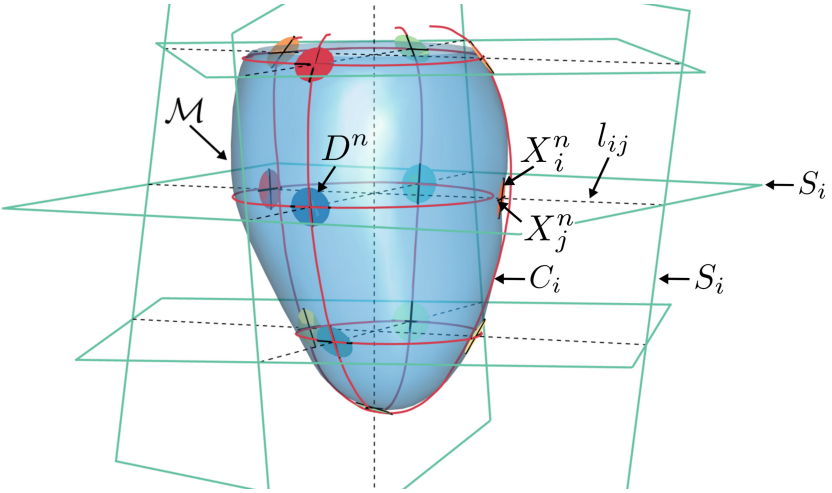

Fig. 1. Illustration of ISACHI definitions.

length $2R$ and lying on S_i. Therefore, $X_i = D^n \bigcap S_i$ only if D^n has been built from S_i. It should be noted that a patch contains 2 segments, belonging to each of the respective intersecting planes, and that there are as many patches as there are intersections between the mesh and line intersections l_{ij}. This is illustrated in Fig. 1.

In order to obtain relevant patches, or slices during our optimization process, we define two functions: $g(n)$ and $p(i)$ that return slice indices when given a patch number, and all the patches built from a specific slice S_i^n, respectively. Let $g(n) = \{i, j\}$ and $p(i) = \{n : i \in g(n)\}$. We now define our energy function to be:

$$J_i = \sum_{n \in p(i)} \sum_{k \in g(n)} \xi(X_k^n, \Psi_k) \tag{1}$$

$$\xi(s, \rho) = \frac{\int_{x \in s} \Psi_x}{2R} \tag{2}$$

where Ψ is the edge map of an image, X_k^n is the $n - th$ segment belonging to slice k, and ξ represents the energy function between a segment and an edge map. The method to compute Ψ is left to the user, and is not detrimental to our method as long as it describes features of interests including edges and borders, which reflect structural information, such as the epicardium and endocardium. The method can work with fundamental techniques such as the magnitude of the gradient, although newer techniques can be used such as the one proposed by [19].

One of our aims is to align slices in order to obtain spatial consistency between the slices and inherently the contours. We assume that slices taken from a subject are triggered at the same cardiac phase and thus there is a global optimal

alignment between the slices which can be modelled by an individual rigid transformation for each slice. We thus consider 3D rigid body transformations with 6 degrees of freedom, represented by: $\theta = \{t_x, t_y, t_z, \alpha, \beta, \gamma\}$. Our optimization can then be defined as: $\underset{\theta_i \in SE(3)}{\operatorname{argmin}} J_i(\theta_i)$, where SE(3) stands for *special Euclidean* and is the set of rigid transformations of dimension 3 and

$$J_i(\theta_i) = \sum_{n \in p(i)} \sum_{k \in g(n)} \xi(s_k^n(\theta_{g(n)}^1, \theta_{g(n)}^2), \theta_k \star \Psi_k) \tag{3}$$

where $\star$ denotes the application of θ on Ψ. Once we have iterated through all the slices until convergence, we consider the slices to be aligned.

We define a global energy

$$\widetilde{J} = \sum_{i=1}^{T} J_i \tag{4}$$

where T is the maximum amount of patches, and inherently the number of intersection points. The Energy J_i represents a measure of how well each of the segments agrees with the image boundary information. It relies on all the segments lying on the slice, as well as the segments lying on the respective intersecting slice. By using the edgeness profiles, calculated from Ψ, the slices can be realigned by taking the information evaluated at the patches.

As the initial contours might not be a correct representation of the segmentation, we proceed to transform individual patches $\{D^n\}$ spatially. As the patches lie on the mesh, which lies close to the non intersecting contours, we consider them to be a good initial approximation of their spatially consistent location. To refine the segmentation independently from slice misalignments, we only allow the patches to move along the intersection lines. In this way, we search for the best spatial location of a patch taking into account the information from its respective intersecting slices. Each patch is optimized iteratively following the same method previously mentioned, but taking into account both intersecting segments. Once the position of the patch has been optimized, the deformation is extrapolated to the contours via approximated thin-plate splines (TPS) [20]. This is to ensure that the patches lie on their optimum calculated positions whilst approximating the mesh in a *smooth* manner

$$\xi_{TPS} = reg(u) + \lambda \sum \|u(m) - F\|^2. \tag{5}$$

where u represents the deformation space, m the moving points ($\{C\}$), F the target points ($D^n(A^*)$), and the operator $\|\cdot\|$ the Frobenius norm. The parameter λ is a smoothing parameter controlling the trade-off between the smoothness of the deformation and the data reliability. Our choice of λ was chosen empirically using a data driven approach. Once deformed, we proceed to recompute a mesh $\mathcal{M}$ to obtain a representation in accordance with the new spatial alignment.

3 Experiments and Results

To properly assess our methodology, synthetic and real data were used. As our algorithm encompasses both alignment and segmentation refinement, synthetic data allowed us to evaluate each component of our method, as we do not possess a *true* spatially consistent clinical ground truth. ISACHI was also applied to a pathological case study, which we present the result for qualitative evaluation. An average MRI heart data obtained from [21][1] was used for our synthetic data. Biventricular average shapes and modes of variation at end-systole and end-diastole are available with their respective surface mesh models. We treated these meshes along with their respective image templates as our ground truth. Using these surface meshes, contours were synthesized by slicing the mesh to form a short axis stack (4 slices), as well as at two (vertical and horizontal) long axis. Random translations and rotations, sampled from uniform distributions with ranges $[-2:2]^\circ$ for each angle and $[-5:5]$ mm for each spatial coordinate were applied to the planes containing the images. Furthermore, non-rigid deformations were applied to the contours to simulate non spatial consistency. For this purpose, eleven uniformly sampled points were extracted from each contour and randomly displaced following a uniform distribution of width 2 mm. The new, deformed, contour points were then calculated using a thin-plate spline interpolation. Using this approach, we generated 10 new cases.

In order to validate the first aspect of our methodology, *i.e.* the ability to correct for slice misalignment, we computed the cross correlation between the line intensities for all slice intersections (as per [6]). This was used as a surrogate measure, assuming that the information at the slice intersection from two slices should be identical. To evaluate the second aspect of our methodology, the accuracy of the segmentation, we applied the iterative closest point (ICP) [22] method between our output mesh and the ground truth mesh, to align them. This allowed to bring the two meshes back to the same spatial location allowing quantitative comparison, in case slices have shifted during optimization. We then compute the average point-to-mesh distance between the two meshes.

The ISACHI algorithm was also applied on real data. A study case having abnormal physiology and severe misalignment was used, and can be seen in Fig. 3. In this case, the slices were initially segmented using our CNN.

3.1 Results

Figure 2 shows a representative result of ISACHI after correcting the misalignments and refining the initial segmentation of the end-diastolic dataset. The slice misalignment for this case ranged from 3–5 mm. Figure 2 shows the mean (red squares), and standard deviations for the normalized cross correlation (NCC) of the intersection line intensities between slices, calculated using the method described in [6], as a function of ISACHI iterations. At the left of the vertical red line is the mean and standard deviation for the NCC values for

[1] http://wp.doc.ic.ac.uk/wbai/data/.

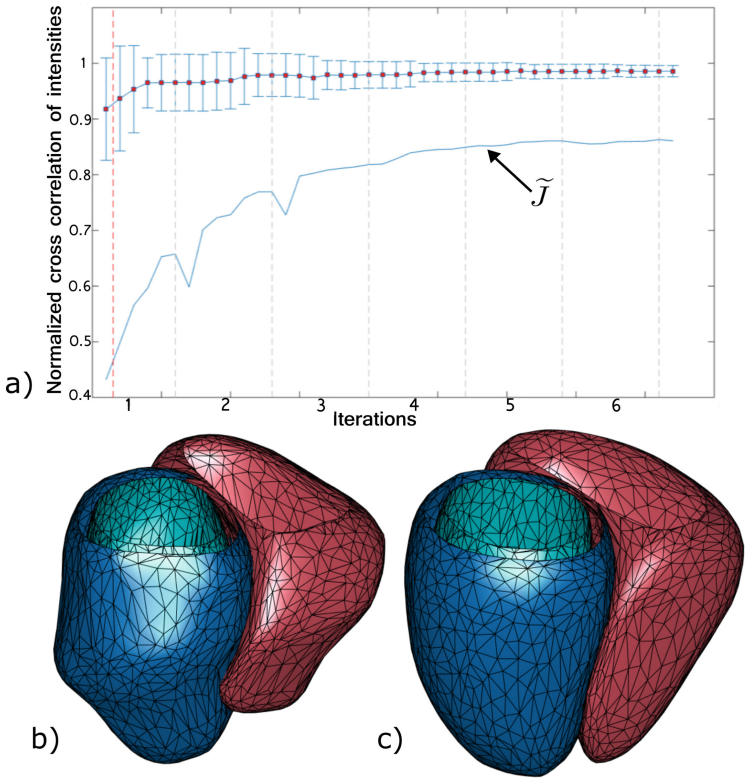

Fig. 2. Alignment correction validation for a representative case. (a) Mean and standard deviation values for the NCC of the intersection line intensities, at every step of ISACHI. The left of the vertical red line represents the synthetically misaligned dataset. The bottom line represents the energy function $\widetilde{J}$. (b) Synthetic mesh: the introduced misalignments are clearly visible. (c) Mesh after ISACHI. (Color figure online)

the misaligned slices. The right of the red line shows the subsequent evaluations for each slice update. The grey vertical lines represent the iterations. In this case, it took 6 iterations to converge. The bottom blue line represents our energy function $\widetilde{J}$. Figure 2(b) shows the mesh generated from the misaligned slices (left) and the result of ISACHI (right). A mesh-to-mesh comparison was performed between the resulting mesh and the ground truth template mesh, between the epi-, endo-, and right ventricle meshes. For the 10 synthetic cases, the mean errors between the misaligned and ground truth meshes were: 2.03 mm, 1.94 mm, 2.20 mm, respectively. After ISACHI, the respective errors were: 1.12 mm, 0.83 mm, 0.83 mm. Figure 3 represents the application of ISACHI on a real case study having abnormal physiology. Figure 3(a) shows the initial CNN segmentation of the slices. The coloured dots in each image correspond to the intersection with a contour on an intersecting slice. In this way, the misalignment between slices can clearly be visualized. Figure 3(c) shows the output of

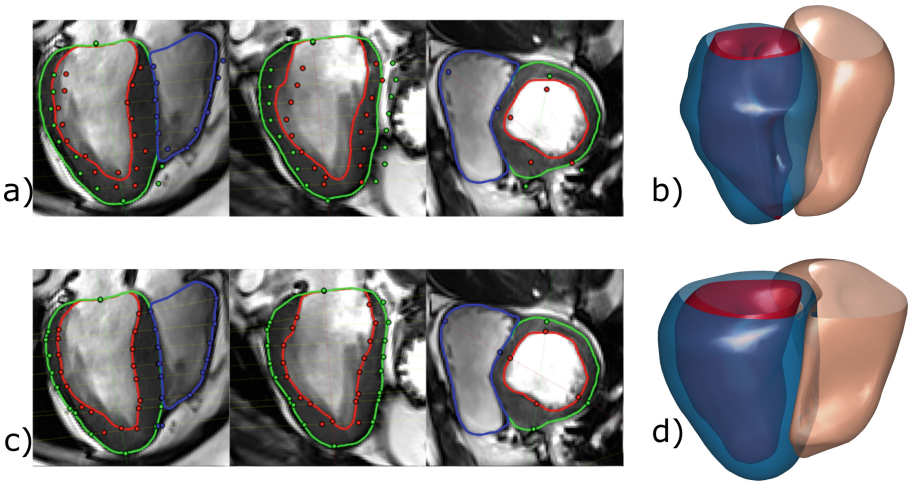

Fig. 3. ISACHI application on abnormal data. (a) The initial CNN segmented data, containing severe misalignment. The coloured dots represent the respective contours from intersecting slices. (b) Mesh reconstructed from the original contours, with the slices at their original locations. (c) The corrected contours and aligned slices. (d) Mesh built from the aligned and deformed contours. (Color figure online)

the algorithm, once the slices have been realigned and the contours deformed to match underlying edges. Finally, Fig. 3(d) shows the resulting corrected mesh, obtained in a fully automated manner.

We presented a novel methodology to perform simultaneous alignment and segmentation correction for cardiac images. Our methodology combines both information from image data as well as consistency in the geometry. The premise of our method lies in that for slices to be aligned, the image features in a slice must match respective features in cross-sectional slices. Furthermore, structural information must also lie on those features of interest. Based on initial slice segmentations, which can be obtained using any method, a surface mesh is generated and used to combine both structural and feature information allowing our optimization to incorporate both global and local data. We show that the method is able to realign the images, as well as recover a realistic mesh. A potential limitation of our method is its reliance on first order patches; it is possible that the use of higher order patches (e.g. quadratic) would improve results.

References

1. Vukicevic, M., Mosadegh, B., Min, J.K., Little, S.H.: Cardiac 3D printing and its future directions. JACC Cardiovasc. Imaging **10**(2), 171–184 (2017)
2. Lopez-Perez, A., Sebastian, R., Ferrero, J.M.: Three-dimensional cardiac computational modelling: methods, features and applications. BioMed. Eng. OnLine **14**(1), 35 (2015)

3. Carminati, M.C., Maffessanti, F., Caiani, E.G.: Nearly automated motion artifacts correction between multi breath-hold short-axis and long-axis cine CMR images. Comput. Biol. Med. **46**, 42–50 (2014)
4. Peng, P., Lekadir, K., Gooya, A., Shao, L., Petersen, S., Frangi, A.: A review of heart chamber segmentation for structural and functional analysis using cardiac magnetic resonance imaging. Comput. Aided Surg. **29**, 155–195 (2016)
5. Ehman, R.L., McNamara, M.T., Pallack, M., Hricak, H., Higgins, C.: Magnetic resonance imaging with respiratory gating: techniques and advantages. Am. J. Roentgenol. **143**(6), 1175–1182 (1984)
6. Villard, B., Zacur, E., Dall'Armellina, E., Grau, V.: Correction of slice misalignment in multi-breath-hold cardiac MRI scans. In: Mansi, T., McLeod, K., Pop, M., Rhode, K., Sermesant, M., Young, A. (eds.) STACOM 2016. LNCS, vol. 10124, pp. 30–38. Springer, Cham (2017). https://doi.org/10.1007/978-3-319-52718-5_4
7. Georgescu, B., et al.: Model based automated 4D analysis for real-time free-breathing cardiac MRI. Proc. Int. Soc. Magn. Reson. Med. (ISMRM) **21**, 4498 (2013)
8. Marchesseau, S., Duchateau, N., Delingette, H.: Segmentation and registration coupling from short-axis cine MRI: application to infarct diagnosis. In: Mansi, T., McLeod, K., Pop, M., Rhode, K., Sermesant, M., Young, A. (eds.) STACOM 2016. LNCS, vol. 10124, pp. 48–56. Springer, Cham (2017). https://doi.org/10.1007/978-3-319-52718-5_6
9. Paiement, A., Mirmehdi, M., Xie, X., Hamilton, M.C.K.: Integrated segmentation and interpolation of sparse data. IEEE Trans. Image Process. **23**(1), 110–125 (2014)
10. Paiement, A., Mirmehdi, M., Xie, X., Hamilton, M.C.K.: Registration and modeling from spaced and misaligned image volumes. IEEE Trans. Image Process. **25**(9), 4379–4393 (2016)
11. Villard, B., Carapella, V., Ariga, R., Grau, V., Zacur, E.: Cardiac mesh reconstruction from sparse, heterogeneous contours. In: Valdés Hernández, M., González-Castro, V. (eds.) MIUA 2017. CCIS, vol. 723, pp. 169–181. Springer, Cham (2017). https://doi.org/10.1007/978-3-319-60964-5_15
12. Villard, B., Grau, V., Zacur, E.: Surface mesh reconstruction from cardiac MRI contours. J. Imaging **4**(1), 16 (2018)
13. Vigneault, D.M., Xie, W., Bluemke, D.A., Noble, J.A.: Feature tracking cardiac magnetic resonance via deep learning and spline optimization. In: Pop, M., Wright, G.A. (eds.) FIMH 2017. LNCS, vol. 10263, pp. 183–194. Springer, Cham (2017). https://doi.org/10.1007/978-3-319-59448-4_18
14. Ronneberger, O., Fischer, P., Brox, T.: U-Net: convolutional networks for biomedical image segmentation. In: Navab, N., Hornegger, J., Wells, W.M., Frangi, A.F. (eds.) MICCAI 2015. LNCS, vol. 9351, pp. 234–241. Springer, Cham (2015). https://doi.org/10.1007/978-3-319-24574-4_28
15. He, K., Zhang, X., Ren, S., Sun, J.: Deep residual learning for image recognition. CVPR (2016)
16. Dolz, J., Desrosiers, C., Ayed, I.B.: 3D fully convolutional networks for subcortical segmentation in MRI: a large-scale study. CoRR abs/1612.03925 (2016)
17. Patravali, J., Jain, S., Chilamkurthy, S.: 2D-3D fully convolutional neural networks for cardiac MR segmentation. CoRR abs/1707.09813 (2017)
18. Zotti, C., Luo, Z., Lalande, A., Humbert, O., Jodoin, P.: Novel deep convolution neural network applied to MRI cardiac segmentation. CoRR (2017)
19. Xie, S., Tu, Z.: Holistically-nested edge detection. In: Proceedings of the 2015 IEEE International Conference on Computer Vision (ICCV), pp. 1395–1403 (2015)

20. Rohr, K., Stiehl, H., Sprengel, R., Buzug, T., Weese, J., Kuhn, M.: Landmark-based elastic registration using approximating thin-plate splines. IEEE Trans. Med. Imaging **20**(6), 526–534 (2001)
21. Bai, W., et al.: A bi-ventricular cardiac atlas built from 1000+ high resolution MR images of healthy subjects and an analysis of shape and motion. Med. Image Anal. **26**(1), 133–145 (2015)
22. Besl, P., McKay, N.: A method for registration of 3-D shapes. IEEE Trans. Pattern Anal. Mach. Intell. **14**(2), 239–256 (1992)